Structure of (001)-, (110)-, and (111)-oriented $Pb(Fe_{1/2}Nb_{1/2})O_3$ epitaxial thin films on $SrRuO_3$-buffered $SrTiO_3$ substrates

Li Yan,[a] Jiefang Li, and D. Viehland
Department of Materials Science and Engineering, Virginia Tech, Blacksburg, Virginia 24061

(Received 31 March 2007; accepted 29 August 2007)

We have studied the lattice structure of variously oriented lead iron niobate (PFN) thin films with thicknesses of $50 < t < 500$ nm that were deposited by pulsed laser deposition (PLD). We have identified that (001)-, (110)-, and (111)-oriented PFN thin films have tetragonal, orthorhombic, and rhombohedral phases at room temperature, respectively. The change in phase stability, when deposited on substrates of different orientations, is discussed with respect to the influence of epitaxial stress.

I. INTRODUCTION

Lead iron niobate, $Pb(Fe_{1/2}Nb_{1/2})O_3$ or PFN, is a relaxor ferroelectric, with a Curie temperature range (or temperature of dielectric maximum, T_{max}) of $T_c \approx 376$ to 393 K.[1–3] The structure of PFN has been an interesting topic since the material was first reported by Smolenskii et al. in 1958.[1] It has been reported that the structure of PFN ceramics is rhombohedral (R) with lattice parameters of $a_r = 4.0123$ Å and $\alpha_r = 89.89°$ in the ferroelectric phase at room temperature, and cubic (C) above T_c in the paraelectric phase.[1,4–6] Later, PFN single crystals were grown, and a ferroelectric → ferroelectric phase transformation was reported at 353K.[7] Using high-resolution x-ray diffraction (XRD), Ehses and Schmid showed that the ferroelectric → ferroelectric transformation was T → R,[8] where the T phase is sandwiched between C and R ones over a narrow temperature region (40 K) on cooling below T_c. The C and T phases are commonly accepted as established; however, in recent years, the existence of the R phase has become more controversial. Bonny et al.[3] and Lampis et al.[9] reported PFN crystals to be monoclinic (M) at room temperature, whereas other neutron[10] and single-crystal[7,8] studies again reported it to be R.

Strontium ruthenate, $SrRuO_3$ (SRO), which is often used as a bottom electrode because of its low resistivity, was first reported by Randall and Ward in 1959.[11–13] At room temperature, bulk SRO has a $GdFeO_3$-type[14] orthorhombic structure with lattice constants of $a_o = 5.5670$ Å, $b_o = 5.5306$ Å, and $c_o = 7.8446$ Å.[15] It can also be seen as a slightly distorted pseudocubic perovskite with single unit-cell lattice constants of $a_{pc} = b_{pc} = c_{pc} = 3.923$ Å, $\alpha = \beta = 90°$, and $\gamma = 89.6°$; or as a pseudo-orthorhombic double unit cell with $a_{po} = 5.57$ Å, $b_{po} = 5.53$ Å, $c_{po} = 3.92$ Å, and $\alpha = \beta = \gamma = 90°$. Strontium titanate, $SrTiO_3$ (STO), is a good choice for a substrate because of its cubic perovskite structure with lattice constant of $a_c = 3.905$ Å at room temperature.

Thin films are known to sometimes have different lattice structures and/or constants, relative to corresponding bulk material forms, due to constraints imposed by substrates. Accordingly, epitaxial films might provide the chance to study the properties of a material in a different crystal structure (or lattice constant) than that available to crystals/ceramics.[16–19] For example, $BiFeO_3$ thin films can be made T, M, or R depending on whether they are deposited on (001), (110), or (111) $SrTiO_3$ substrates.[18,19] Previously, several papers have been published on PFN thin films deposited by sol-gel,[20–22] pulsed laser deposition (PLD),[23–25] and sputtering.[26] However, the structure of PFN thin layers has not previously been reported.

Here, we report an investigation of the crystal structures of variously oriented PFN epitaxial thin films grown on $SrRuO_3$-coated $SrTiO_3$ by PLD. We find that (001), (110), and (111) layers are T, O, and R, respectively. The dielectric and ferroelectric properties of these three phases, some of which do not exist in PFN crystals/ceramics, are compared. The dependence of lattice parameters on film thickness is also given.

II. EXPERIMENTAL PROCEDURE

To ensure the stoichiometric ratio of different ions, targets of PFN were prepared using a one-step solid-state reaction method. Powders of PbO (99.9%), Fe_2O_3 (99.945%), and Nb_2O_5 (99.9%) were batched in stoichiometric ratio, with an excess of 5% PbO. After 3 h

[a]Address all correspondence to this author.
e-mail: lyan@vt.edu
DOI: 10.1557/JMR.2008.0081

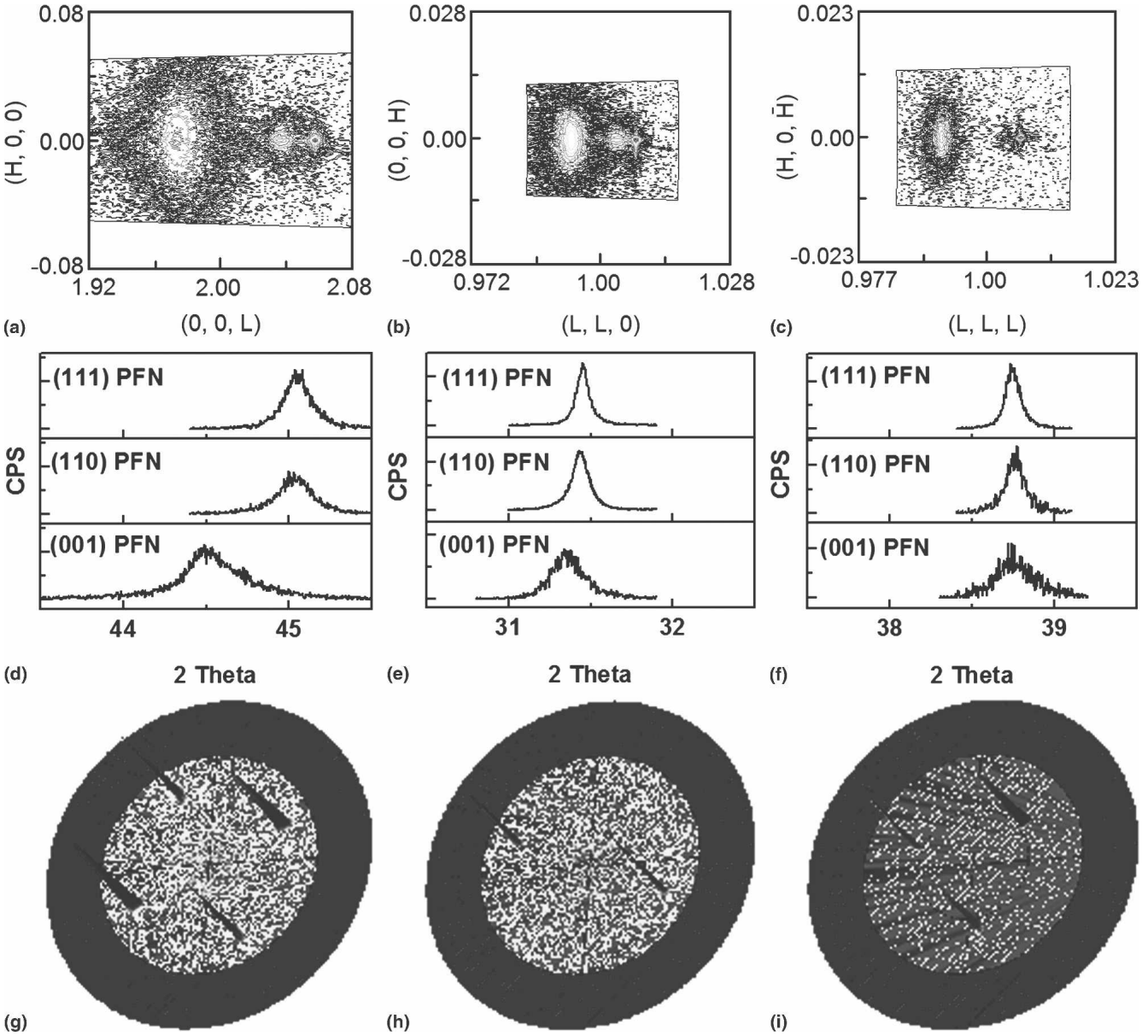

FIG. 1. XRD results: mesh scans, line scans, and pole-figure scans of PFN thin films. (a) Mesh scan of (002) PFN/SRO/STO for (001)-oriented film. (b) Mesh scan of (110) PFN/SRO/STO for (110)-oriented film. (c) Mesh scan of (111) PFN/SRO/STO for (111)-oriented film, demonstrating phase purity and good epitaxy. (d) Line scan of (002) peaks for (001)-, (110)-, and (111)-oriented films. (e) Line scan of (110) peaks for (001)-, (110)-, and (111)-oriented films. (f) Line scan of (111) peaks for (001)-, (110)-, and (111)-oriented films, which are used to determine the lattice constants of PFN thin films. (g) Pole-figure scan of {101} peaks about ⟨001⟩ axis for (001)-oriented PFN film. (h) Pole-figure scan of {100} peaks about ⟨110⟩ axis for (110)-oriented PFN film. (i) Pole-figure scan of {110} peaks about ⟨111⟩ axis for (111) oriented PFN film, demonstrating the symmetry of the PFN films.

calcination at 850 °C, samples were sintered for 3 h at 920 °C by controlled-atmosphere sintering to reduce Pb loss. Epitaxial thin films of PFN were subsequently deposited by PLD using these targets. Deposition was done on (001)-, (110)-, and (111)-oriented STO substrates. The energy density of the KrF laser (Lambda 305i) (Lambda Physik, Inc., Blacksburg, VA) was 1.6 J/cm^2 at a wavelength of 248 nm. The distance between the target and substrate was 6 cm. The growth rate of the PFN thin films was, for example, 10 nm/min at a deposition temperature of 630 °C. A 50 nm SRO layer was used as a buffer layer, which was deposited by PLD at 650 °C using a growth rate of 0.7 nm/min. PFN thin films of various thicknesses were grown from $50 < t < 500$ nm.

The structural and ferroelectric properties of the thin films were measured. XRD studies were performed using a Philips X'pert (PANalytical, Blacksburg, VA) high-resolution system equipped with a two-bounce hybrid

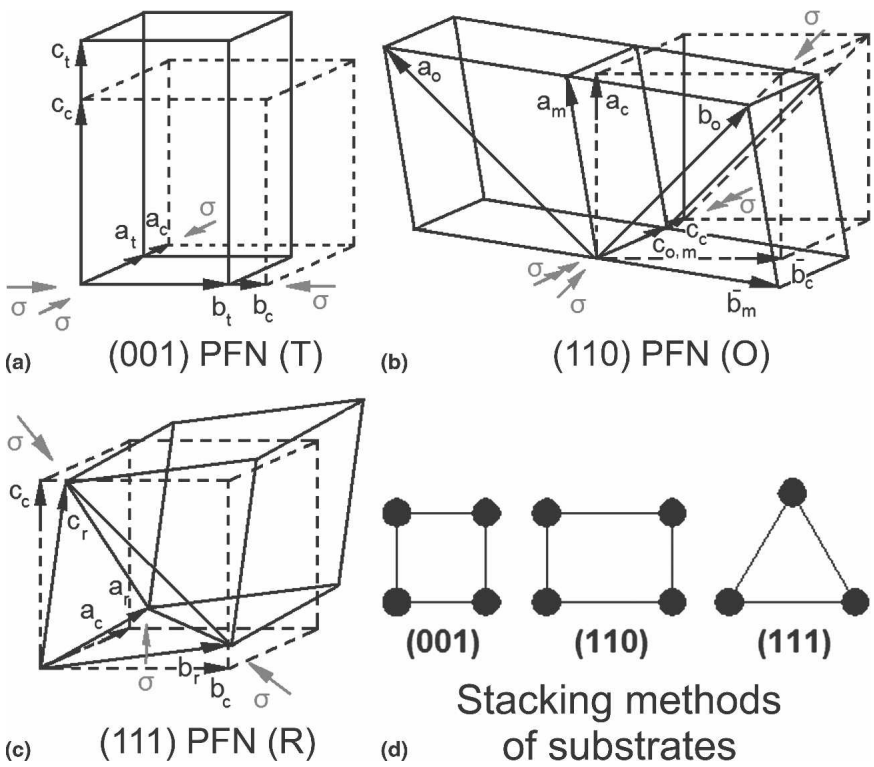

FIG. 2. Structure and stress of various oriented PFN films. (a) Tetragonal structure of (001)-oriented PFN film, and stress along ⟨100⟩ and ⟨010⟩ directions. (b) Orthorhombic (or monoclinic) structure of (110)-oriented PFN film, and stress along ⟨1$\bar{1}$0⟩ and ⟨010⟩ directions. (c) Rhombohedral structure of (111)-oriented PFN film, and stress in (111) plane. (d) Stacking method on the surfaces of the variously oriented substrates.

monochromator, and an open three-circle Eulerian cradle. The analyzer was a Ge (220) cut crystal that had a θ resolution of 0.0068°. The x-ray unit was operated at 45 kV and 40 mA with a wavelength of 1.5406 Å (Cu K_α). Line, mesh, and pole-figure scans were obtained to ensure proper identification of the lattice structure of the variously oriented PFN thin films. The (002) and (004), (110) and (220), and (111) and (222) peaks of a STO single crystal were used to calibrate the offset of the XRD unit. The Gauss method was used to approach the position of the peak in the calculation of the lattice constants of PFN, SRO, and STO.

III. RESULTS AND DISCUSSION

A. Crystal structure and lattice parameters of various oriented PFN film at room temperature

Figures 1(a)–1(c) show mesh scans for (001)-, (110)-, (111)-oriented PFN/SRO/STO heterostructures. We can see that the PFN films are phase-pure perovskite that are epitaxial with STO. The residual stress of the (111) oriented film is less than that of the (110) film, the stress of which is less than that of the (001) oriented film. Line scans for the (002), (110), and (111) peaks are shown in Figs. 1(d), 1(e), and 1(f), respectively: each figure contains data for (001)-, (110)-, and (111)-oriented PFN thin films. Analysis of these x-ray data allowed for the determination of the structure and lattice parameters of the various oriented films

The structure of the (001)-oriented PFN thin film is tetragonal [see Fig. 2(a)], which is the same as that of the intermediate ferroelectric phase of bulk PFN crystals/ceramics in the temperature range of 353 and 393 K. The lattice parameter c_t was 4.068 Å for a 100 nm thick PFN layer as determined from the (002) peak, and a_t was determined to be 4.010 Å by analysis of the (002) and (101) peaks. The value of $d_{(111)}$ was then used to verify the value of the lattice parameters c_t and a_t, whose result was a match. The four values of $d_{\{101\}}$ were nearly equivalent, where the error difference was smaller than the resolution of the XRD system. Furthermore, for a tetragonal structure, the ⟨001⟩ (i.e., *c*-axis) must be a fourfold rotation axis. Figure 1(g) shows a pole-figure scan of the {101} peaks about the same ⟨001⟩ axis for a (001)-oriented PFN film. Accordingly, there are four equivalent {110} peaks, with nearly the same intensity, which are rotated from each other by an angle of $\phi = 90°$. These results clearly confirm that the *c*-axis of the PFN film is fixed by the (001) axis of the substrate and that there are four equivalent {101} planes consistent with a tetragonal structure.

The structure of the (110)-oriented PFN thin films was a double-cell orthorhombic, or equivalently a limiting monoclinic C (M_c) single-cell representation, as shown

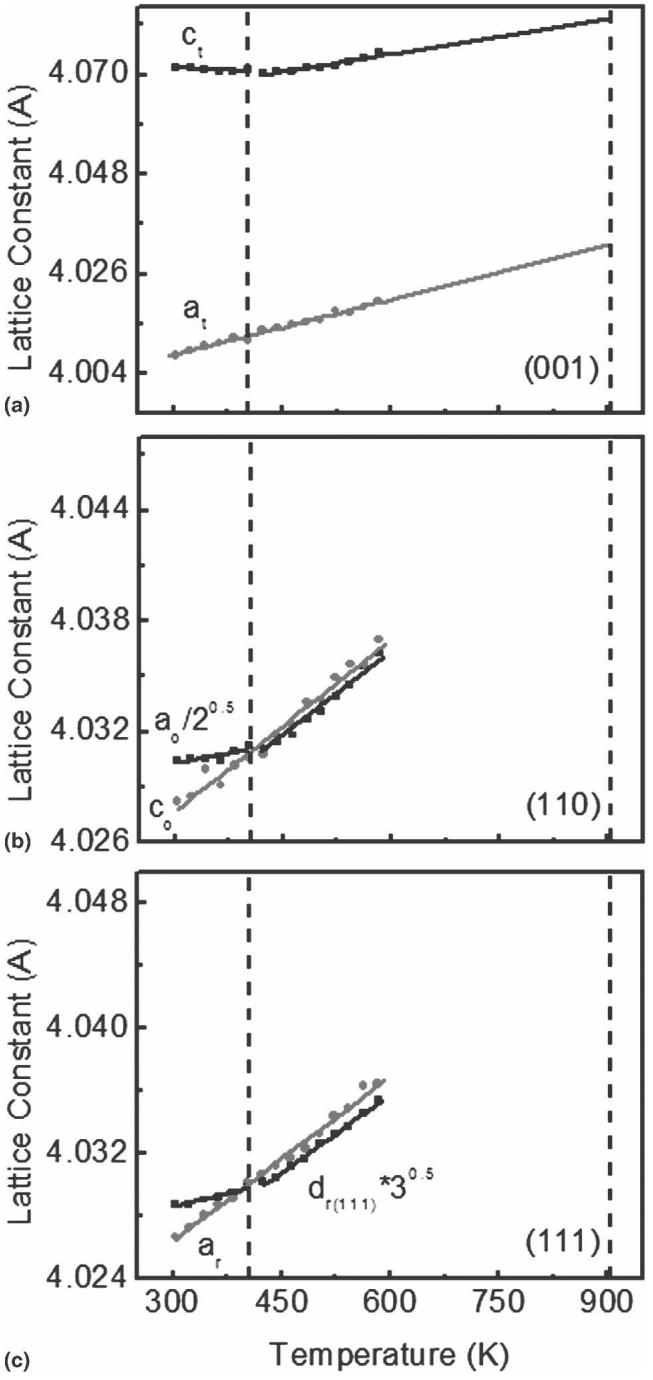

FIG. 3. Lattice parameters of various orientated PFN films as a function of temperature. (a) a_t and c_t lattice parameters of (001) PFN film as a function of temperature, demonstrating T → T′ phase transition. (b) $a_o/\sqrt{2}$ and c_o lattice parameters of (110) PFN film as a function of temperature, demonstrating C → O phase transition. (c) $d_{r(111)}/\sqrt{3}$ and a_r lattice parameters of (111) PFN film as a function of temperature, demonstrating C → R phase transition.

in Fig. 2(b). The O phase has not been previously reported in PFN crystal or ceramics. For the single-cell representation, we determined the M_c lattice parameters for a 100-nm-thick PFN film to be $a_m = b_m = 4.029$ Å and $\gamma = 89.93°$ by analysis of (200) and (110) peaks, and $c_m = 4.017$ Å by analysis of (110) and (111) peaks. Whereas in double-cell representation, the lattice constants of the O phase were determined to be (a_o, b_o, c_o) = (5.702 Å, 5.694 Å, 4.017 Å). These representations are equivalent, and in this paper we chose to refer to the higher symmetry O structure. Figure 1(h) shows a pole-figure scan of the {200} peaks taken about the ⟨110⟩ axis of a (110) oriented PFN thin film: two {200} peaks with equal intensity, which are rotated by $\phi = 180°$, can be seen consistent with the O structure. For PFN single crystals, Bonny et al. has also reported a monoclinic phase with a double cell at 297 K.[3] The difference between the O phase for (110) oriented PFN thin films and the M phase for single crystal is the angle β, which was 90.1° for the crystal (i.e., the M was a slightly distorted O structure).

The structure of the (111) oriented PFN thin film was R, as illustrated in Fig. 2(c), which was the same as that of PFN crystals/ceramic at room temperature. From analysis of (200) and (110) peaks, we determined that $a_r = b_r = c_r = 4.027$ Å and $\alpha = 89.96°$ for a 100 nm thick PFN layer. These same values were also confirmed by analysis of (200) and (111) peaks. Pole-figure scans of the {110} peaks around about the ⟨111⟩ axis for a (111) oriented film revealed a threefold axis of rotation as shown in Fig. 1(i). The facts that $d_{(200)} = d_{(020)} = d_{(002)}$ and that there was threefold {110} pole scan prove that (111) PFN films are R.

B. Structure of PFN thin films: Role of epitaxial stress and lattice mismatch

The reason why the T phase with $c_t/a_t = 1.015$ is favored for (001) PFN layers is shown in Fig. 2(a). An axial compressive stress acts along the ⟨100⟩ and ⟨010⟩ direction on the (001) face between the PFN film and the (001) SRO/STO substrate. The structure is similar to the intermediate phase of PFN single crystals in the temperature range of 353 to 393 K, but has a change in c_t/a_t caused by epitaxial constraint. If the film was stress free in all directions and if there was no striction associated with any phase transformations, then the lattice parameters would be $a_c = b_c = c_c \approx 4.028$ Å at room temperature. However, the lattice parameter of SRO is $a_c = 3.923$ Å, which is smaller than that of PFN. Thus, the a_t and b_t lattice parameters of PFN thin films are compressed equally to 4.010 Å, and c_t expanded to 4.068 Å. The tetragonal cell volume is nearly equivalent to that of the presumed C, as $a_t^2 c_t = a_c^3 = 65.4$ Å^3.

The reason why the O phase is favored for (110) films is that an anisotropic stress acts along the ⟨001⟩ and ⟨1$\bar{1}$0⟩ directions on the (110) face between the PFN film and SRO/STO substrate, as illustrated in Fig. 2(b). Since in the (110) plane the compressive stress along $\langle 001\rangle_c$ is larger than that along $\langle 110\rangle_c$ in the (110) plane, b_o is

compressed from 5.698 to 5.694 Å by the stress acting along $\langle 1\bar{1}0\rangle_c$, c_o is compressed from 4.028 to 4.017 Å by the $\langle 001\rangle_c$ stress, and a_o expands from 5.698 to 5.702 Å.

The (111) film is R, similar to crystals/ceramics. An isotropic compressive stress is applied by the (111) SRO/STO substrate on the PFN film, as shown in Fig. 2(c). Accordingly, (111) PFN thin films cannot change their crystal structure, and the R phase is maintained. Interestingly, the R lattice parameters of the film are larger (a_r = 4.027 Å) than those previously reported for PFN crystals (a_r = 4.012 Å); however, the cell volume of the film is nearly equal to that of the presumed C structure ($a_r^3 \sin\alpha_r = a_c^3$ = 65.4 Å^3).

The constraint stresses are different for the variously oriented films because of the different stacking patterns on the substrate surfaces, as illustrated in Fig. 2(d). The stacking patterns on the (001), (110), and (111) SRO/STO substrate surfaces are square, rectangular, and triangular, respectively. Although the lattice constant of PFN is slightly larger (2% to ~4%) than that of SRO, PFN grew epitaxially on SRO/STO substrates. Thus, a constraint stress is generated, and the stresses are different for the variously oriented substrates.

C. Phase transformational sequences with temperature

The dependence of the lattice parameters of a 150 nm thick (001) oriented PFN thin film on temperature is shown in Fig. 3(a). In this figure, we can see a change in the slope of the thermal expansion near 400 K, which is close to the T_c previously reported for crystals/ceramics. The lattice parameters in both the high- and low-temperature phases were tetragonal. Thus, we designate the transformational sequence as T → T′, where presumably T is paraelectric and T′ is ferroelectric. A tetragonal distortion of c_t/a_t = 4.014 persists to 600 K, whose linear extrapolation to the deposition temperature of 900 K yields c_t/a_t = 1.012. This demonstrates that a tetragonal distortion was induced by epitaxial stress from the substrate during the film formation, rather than by a consequence of a ferroelectric phase transformation.

However, for the (110) and (111) oriented PFN thin films, the structural distortions from the cubic prototype are a direct consequence of a ferroelectric transformation. The dependence of the lattice parameters for 150 nm thick (110) and (111) PFN thin films on temperature are shown in Figs. 3(b) and 3(c). In these figures, we can again see a change in slope of the thermal expansion at a Curie temperature of $T_c \approx 400$ K, which corresponds to that of crystals/ceramics.[1,2] In both cases, the high-temperature phase is cubic. However, the structures of the low-temperature ferroelectric phases were different: (110) was O, and (111) was R. The values of the lattice parameters in both cases were quite similar over the entire temperature range.

D. Thermal expansion of PFN thin films

The volumetric/linear thermal expansion coefficients (TECs) (β/α) of STO and PFN that were previously reported in the literature are summarized in Table I. The volumetric TEC of STO is constant (3.23×10^{-5} K^{-1}) over a wide temperature range (300 to ~2000 K).[27–29] For PFN, the volumetric TEC changes considerably both below and above the Curie temperature. The value of the volumetric coefficient β1 is 0.36×10^{-5} K^{-1} between room temperature and T_c; whereas for temperatures above T_c, β2 increases to 3.3×10^{-5} K^{-1},[30–32] becoming nearly equal to the value of STO.

TABLE I. Thermal expansion coefficient (TEC) of STO substrate and PFN thin films.

Volumetric TEC	β (10^{-5} K^{-1})	ΔT (K)			References
STO	2.82	110–300			27
	2.59	113–301			28
	3.23	300–2000			29
	3.18	303–583			This study
Volumetric TEC	**β1 (10^{-5} K^{-1})**	**ΔT (K)**	**β2 (10^{-5} K^{-1})**	**ΔT (K)**	**References**
Bulk PFN	0.318	RT			30
	0.288	300–385	3.828	445–800	31
	0.36	300–393	3.3	>393	32
(001) PFN film	1.96	303–383	2.88	463–583	This study
(111) PFN film	2.37	303–383	3.19	463–583	This study
Linear TEC	**α (10^{-5} K^{-1})**	**ΔT (K)**			**References**
a_t of (001) PFN film	1.01	303–583			This study
c_o of (110) PFN film	0.981	303–583			This study
$d_{r(10\bar{1})}$ of (111) PFN film	1.02	303–583			This study
STO substrate	1.06	303–583			This study

RT, room temperature.

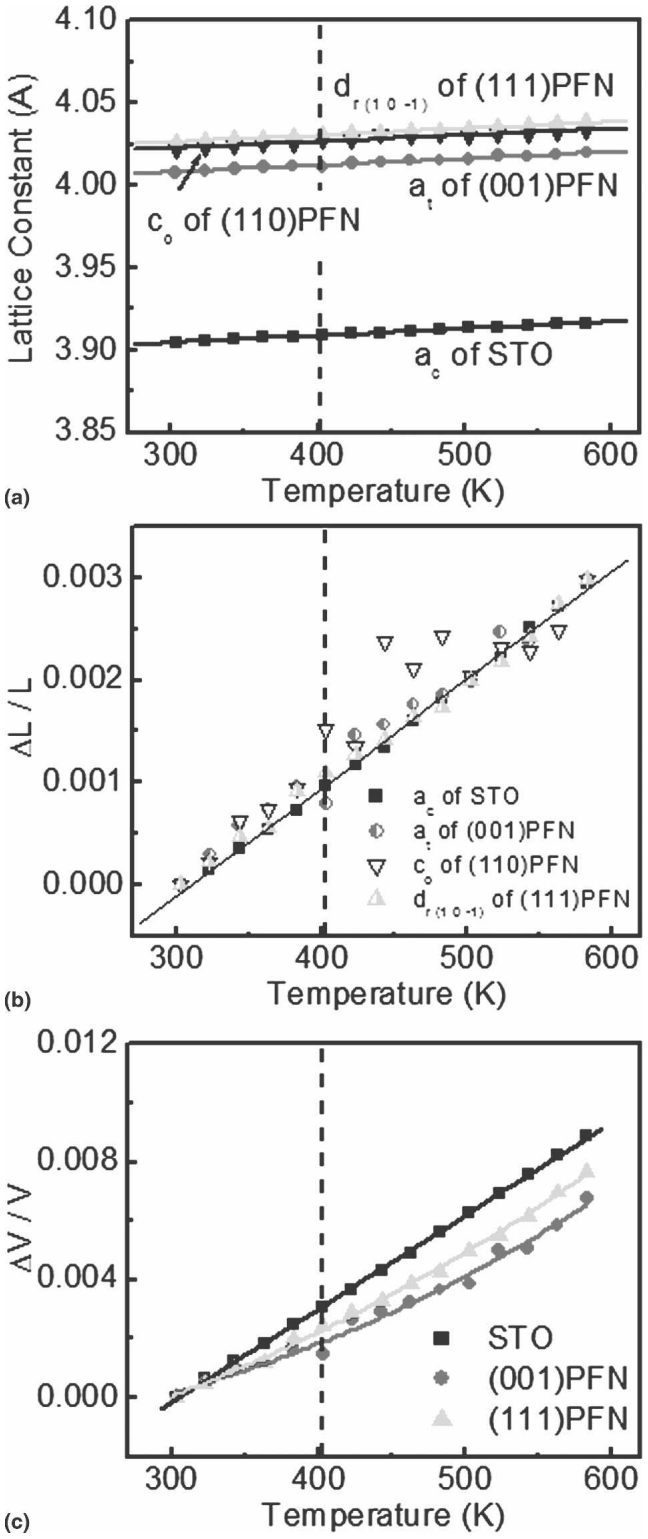

FIG. 4. Thermal expansion of various oriented PFN thin films and STO substrate as a function of temperature. (a) In-plane lattice constants of PFN thin films [a_t of (001) PFN films, c_o of (110) PFN thin films, and $d_{r(10\bar{1})}$ of (111) PFN thin films] and lattice constant of STO substrate as a function of temperature. (b) $\Delta L/L$ of in-plane lattice constant of PFN thin films and STO substrate as a function of temperature. (c) $\Delta V/V$ of PFN thin films and STO substrate as function of temperature.

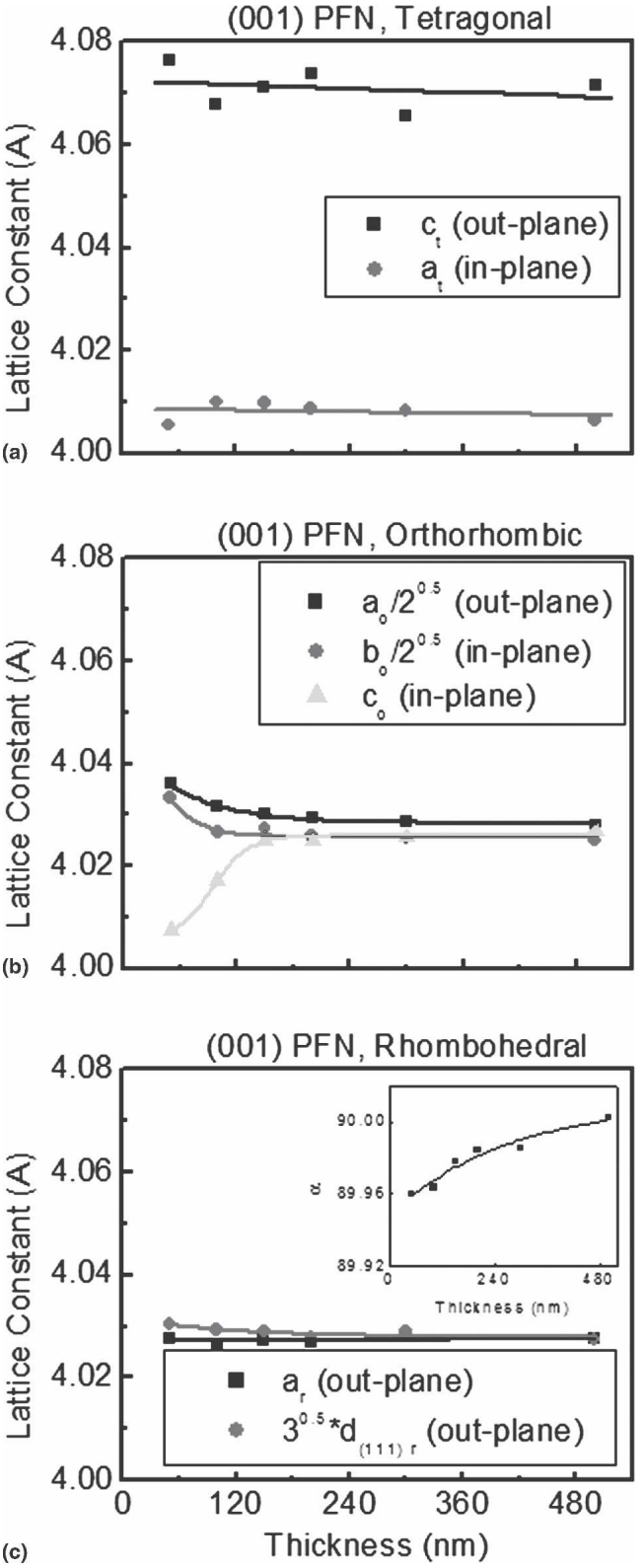

FIG. 5. Lattice parameters of various orientated PFN films as a function of film thickness. (a) a_t and c_t lattice parameters of (001) PFN film as a function of film thickness. (b) $a_o/\sqrt{2}$, $b_o/\sqrt{2}$ and c_o lattice parameters of (110) PFN film as a function of film thickness. (c) $d_{r(111)}/\sqrt{3}$ and a_r lattice parameters of (111) PFN film as a function of film thickness, where the insets shows α.

To study the thermal expansion of PFN thin films and STO substrate, the in-plane and out-plane lattice constants of PFN films and the lattice constant of STO were measured from 303 to 583 K. As shown in Fig. 4(a), the lattice constant a_t of (001), c_o of (110), and $d_{r(10\bar{1})}$ of (111) PFN thin films increased near-linearly with increasing temperature. Over the temperature range investigated, the mismatch between the in-plane lattice constants of PFN thin films and that of the STO substrate was essentially constant. Accordingly, this shows that the strain between the PFN film and substrate are also unchanged on heating in the range of 303 to 583 K. The values of $\Delta L/L$ between the in-plane lattice constant of PFN films and that of the STO substrate are shown in Fig. 4(b) as a function of temperature. As can be seen in this figure, the linear TEC of the in-plane lattice constants for PFN films and that of the STO substrate are nearly the same in the temperature range between 303 and 583 K. Values of the linear TEC for the in-plane lattice constant of PFN (1×10^{-5} K^{-1}) are then summarized in Table I, where they can be seen to be similar to those for STO (1.06×10^{-5} K^{-1}). Because of the elastic constraint imposed by the SRO/STO substrate, the linear TEC of the in-plane lattice constant of PFN films both below and above Curie temperature is constant: this is notably different with that of bulk PFN crystals and ceramics.

The thermal expansion volume for each PFN film was then calculated as a function of temperature, using the lattice constants. The values of $\Delta V/V$ for the (001) and (111) PFN films and the STO substrate are shown in Fig. 4(c) as a function of temperature. For the PFN films at temperatures above T_c, the volumetric TEC was 3×10^{-5} K^{-1} which was about the same as that of STO, whereas below T_c, it had a lower value of 2×10^{-5} K^{-1}, which is still notably larger than that of bulk PFN. The reason for the reduction in the volumetric TEC of PFN films is probably the change in the out-plane lattice constant below T_c. Because of the epitaxial constraint imposed by the substrate, the volumetric thermal expansion of PFN cannot be as small as that of bulk PFN.

E. Thickness dependence of lattice parameters

The dependence of the lattice parameter for (001) PFN thin films on film thickness is shown in Fig. 5(a). These films were all tetragonal, and the lattice parameters were nearly independent of film thickness. These results demonstrate that the epitaxial stress in (001) films is not relaxed with increasing film thickness (at least for $t \leqslant 500$ nm).

However, for the (110) and (111) films, the lattice parameters were notably dependent on film thickness. For the (110) film, Fig. 5(b) shows that $a_o/\sqrt{2}$ and $b_o/\sqrt{2}$ both decreased with increasing film thickness for $t \leqslant 150$ nm, whereas c_o increased. Near $t = 150$ nm, the structure appears pseudocubic with $a_o/\sqrt{2} \approx b_o/\sqrt{2} \approx c_o$. The reason for the thinner films having $a_o/\sqrt{2}$ and $b_o/\sqrt{2}$ larger than c_o is that the compressive stress along $\langle 001 \rangle$ is larger than that along $\langle 1\bar{1}0 \rangle$ in the (110) plane. The results show for (110) PFN that increasing film thickness relaxes the epitaxial stress, accordingly the orthorhombic distortion of the structure is reduced. Similarly, the small R distortion of the (111) PFN thin layers was reduced with increasing film thickness, as shown in Fig. 5(c). In fact, the structure of the thicker (111) films was seemingly pseudocubic.

IV. SUMMARY

Our structural investigations demonstrate that the phase transformational sequence of PFN thin films grown on $SrRuO_3$-coated $SrTiO_3$ substrates depends on orientation:

(1) T → T′ for (001) layers,
(2) C → O for (110) layers, and
(3) C → R for (111) ones.

The O and T′ phases do not exist in bulk PFN crystals/ceramics at room temperature. The change in transformational sequence with orientations is attributed to epitaxial stress.

ACKNOWLEDGMENT

We would like to gratefully acknowledge financial support from the United States Department of Energy under Contract No. DE.-AC02-98CH10886, and the Air Force Office of Scientific Research under FA 9550-06-1-0410.

REFERENCES

1. G.A. Smolenskii, A. Agranovskaya, S.N. Popov, and V.A. Isupov: New ferroelectrics of complex composition. *Sov. Phys. Tech. Phys.* **28,** 2152 (1958, in Russian).
2. G.L. Platonov, L.A. Drobyshev, Y.Y. Tomashpolskii, and Y.N. Venevtsev: Electron-diffraction and x-ray-diffraction investigation of atomic displacements in ferromagnet $Pb(Fe_{0.5}Nb_{0.5})O_3$. *Sov. Phys. Crystallogr.* **14,** 692 (1970).
3. V. Bonny, M. Bonin, P. Sciau, K.J. Schenk, and G. Chapuis: Phase transitions in disordered lead iron niobate: X-ray and synchrotron radiation diffraction experiments. *Solid State Commun.* **102,** 347 (1997).
4. V.A. Vokov, I.E. Mylnikova, and G.A. Smolenskii: *Sov. Phys. JETP* **15,** 447 (1962).
5. Y. Yang, J.M. Liu, H.B. Huang, W.Q. Zou, P. Bao, and Z.G. Liu: Magnetoelectric coupling in ferroelectromagnet $Pb(Fe_{1/2}Nb_{1/2})O_3$ single crystals. *Phys. Rev. B* **70,** 132101 (2004).
6. Y. Yang, S.T. Zhang, H.B. Huang, Y.F. Chen, Z.G. Liu, and J.M. Liu: Microstructural characterizations of ferroelectromagnet lead iron niobate crystals. *Mater. Lett.* **59,** 1767 (2005).
7. I.H. Brunskill, R. Boutellier, W. Depmeier, H. Schmid, and H.J. Scheel: High-temperature solution growth of $Pb(Fe_{0.5}Nb_{0.5})O_3$ and $Pb(Mn_{0.5}Nb_{0.5})O_3$ crystals *J. Cryst. Growth* **56,** 541 (1982).
8. K.H. Ehses and H. Schmid: The high temperature phase transitions of $Pb(Nb_{0.5}Fe_{0.5})O_3$. *Z. Kristallogr.* **162,** 64 (1983).
9. N. Lampis, P. Sciau, and A.G. Lehmann: Rietveld refinements of

the paraelectric and ferroelectric structures of $PbFe_{0.5}Nb_{0.5}O_3$. *J. Phys. Condens. Matter.* **11,** 3489 (1999).
10. S.A. Ivanov, R. Tellgren, H. Rundlof, N.W. Thomas, and S. Ananta: Investigation of the structure of the relaxer ferroelectric $Pb(Fe_{1/2}Nb_{1/2})O_3$ by neutron powder diffraction. *J. Phys.: Condens. Matter* **12,** 2393 (2000).
11. J.J. Randall and R. Ward: The preparation of some ternary oxides of the platinum metals. *J. Am. Chem. Soc.* **81,** 2629 (1959).
12. R.J. Bouchard and J.L. Gillson: Electrical properties of $CaRuO_3$ and $SrRuO_3$ single crystals. *Mat. Res. Bull.* **7,** 873 (1972).
13. C.B. Eom, R.J. Cava, R.M. Fleming, J.M. Phillips, R.B. van Dover, J.H. Marshall, J.W.P. Hsu, J.J. Krajewski, and W.F. Peck, Jr.: Single-crystal epitaxial thin films of the isotropic metallic oxides $Sr_{1-x}Ca_xRuO_3$ ($0 \leqslant x \leqslant 1$). *Science* **258,** 1766 (1992).
14. S. Geller: Crystal structure of gadolinium orthoferrite, $GdFeO_3$. *J. Chem. Phys.* **24,** 1236 (1956).
15. C.W. Jones, P.D. Battle, and P. Lightfoot: The structure of $SrRuO_3$ by time-of-flight neutron powder diffraction. *Acta Crystallogr.* **C45,** 365 (1989).
16. B.A. Tuttle, T. Headley, C. Drewien, J. Michael, J. Voigt, and T. Garino: Comparison of ferroelectric domain assemblages in $Pb(Zr,Ti)O_3$ thin films and bulk ceramics. *Ferroelectrics* **221,** 209 (1999).
17. G.L. Brennecka, W. Huebner, B.A. Tuttle, and P.G. Clem: Use of stress to produce highly oriented tetragonal lead zirconate titanate (PZT 40/60) thin films and resulting electrical properties. *J. Am. Ceram. Soc.* **87,** 1459 (2004).
18. J. Li, J. Wang, M. Wuttig, R. Ramesh, N. Wang, B. Ruette, A.P. Pyatakov, A.K. Zvezdin, and D. Viehland: Dramatically enhanced polarization in (001), (101), and (111) $BiFeO_3$ thin films due to epitaxial-induced transitions. *Appl. Phys. Lett.* **84,** 5261 (2004).
19. G.Y. Xu, H. Hiraka, G. Shirane, J. Li, J. Wang, and D. Viehland: Low symmetry phase in (001) $BiFeO_3$ epitaxial constrained thin film. *Appl. Phys. Lett.* **86,** 182905 (2005).
20. M. Sedlar and M. Sayer: Study of electrical properties of rapid thermal processed lead iron niobate films synthesized by a sol gel method. *J. Appl. Phys.* **80,** 372 (1996).
21. M. Sedlar, M. Sayer, and D.T. Amm: Leakage current in rapid thermally processed lead iron niobate films synthesized by a sol gel method. *J. Appl. Phys.* **80,** 367 (1996).
22. Q. Liu, G.H. Yi, and D.J. Barber: Oriented nano-structured $Pb(Fe_{0.5}Nb_{0.5})O_3$ thin films on $SrTiO_3$(100) substrates by a sol-gel technique. *Mater. Lett.* **38,** 239 (1999).
23. X.S. Gao, X.Y. Chen, J. Yin, J. Wu, Z.G. Liu, and M. Wang: Ferroelectric and dielectric properties of ferroelectromagnet $Pb(Fe_{1/2}Nb_{1/2})O_3$ ceramics and thin films. *J. Mater. Sci.* **35,** 5421 (2000).
24. X.R. Wang, S.S. Fan, Q.Q. Li, B.L. Gu, and X.W. Zhang: Fabrication of lead iron niobate films on Si substrate by pulsed laser deposition. *Jpn. J. Appl. Phys.* **35,** L1002 (1996).
25. X.R. Wang, S.S. Fan, Q.Q. Li, B.L. Gu, and X.W. Zhang: Study on microstructure and interdiffusion behavior in $Pb(Fe_{1/2}Nb_{1/2})O_3$/Pt/Ti/SiO_2/Si(100) multilayer films. *Mater. Res. Bull.* **32,** 1247 (1997).
26. C.V. Kumar, M. Sayer, and R. Pascual: Fabrication of modified lead iron niobate films. *Appl. Phys. Lett.* **60,** 2080 (1992).
27. F.W. Lytle: X-ray diffractometry of low-temperature phase transformations in strontium titanate. *J. Appl. Phys.* **35,** 2212 (1964).
28. K. Itoh, K. Ochiai, H. Kawaguchi, C. Moriyoshi, and E. Nakamura: Structural fluctuations of $SrTiO_3$ in the cubic phase. *Ferroelectrics* **159,** 85 (1994).
29. D. de Ligny and P. Richet: High-temperature heat capacity and thermal expansion of $SrTiO_3$ and $SrZrO_3$ perovskites. *Phys. Rev. B* **53,** 3013 (1996).
30. M. Yokosuka: Electrical and electromechanical properties of hot-pressed $Pb(Fe_{1/2}Nb_{1/2})O_3$ ferroelectric ceramics. *Jpn. J. Appl. Phys.* **32,** 1142 (1993).
31. M.V. Radhika Rao and A.M. Umarji: Thermal expansion studies in lead iron niobate–lead zinc niobate and related systems. *Mater. Res. Bull.* **30,** 1031 (1995).
32. V.V.S.S. Sai Sunder and A.M. Umarji: Thermal expansion studies in the lead iron niobate–lead titanate system. *Mater. Res. Bull.* **30,** 427 (1995).